

---

This is an electronic reprint of the original article.  
This reprint may differ from the original in pagination and typographic detail.

Wang, Jing; Wang, Heqi; Wang, Chunguang

## Optimal Charging Pile Configuration and Charging Scheduling for Electric Bus Routes Considering the Impact of Ambient Temperature on Charging Power

*Published in:*  
Sustainability

*DOI:*  
[10.3390/su15097375](https://doi.org/10.3390/su15097375)

Published: 28/04/2023



*Document Version*  
Publisher's PDF, also known as Version of record

*Published under the following license:*  
CC BY

*Please cite the original version:*  
Wang, J., Wang, H., & Wang, C. (2023). Optimal Charging Pile Configuration and Charging Scheduling for Electric Bus Routes Considering the Impact of Ambient Temperature on Charging Power. *Sustainability*, 15(9), Article 7375. <https://doi.org/10.3390/su15097375>

## Article

# Optimal Charging Pile Configuration and Charging Scheduling for Electric Bus Routes Considering the Impact of Ambient Temperature on Charging Power

Jing Wang <sup>1</sup> , Heqi Wang <sup>2</sup> and Chunguang Wang <sup>3,\*</sup> 

<sup>1</sup> College of Engineering, Shenyang Agricultural University, Shenyang 110866, China; wj77@syau.edu.cn

<sup>2</sup> Department of Built Environment, Aalto University, 01250 Espoo, Finland; heqi.wang000@gmail.com

<sup>3</sup> State Key Laboratory for Strength and Vibration of Mechanical Structures, School of Aerospace Engineering, Xi'an Jiaotong University, Xi'an 710049, China

\* Correspondence: wangchunguang@xjtu.edu.cn

**Abstract:** Charging piles in the bus depot provide charging services to multiple electric bus (EB) routes operating in the area. As charging needs may overlap between independently operated routes, EB fleets often have to wait in line for charging. However, affected by the ambient temperature, the length of the waiting time will cause the battery temperature to change at the beginning of each charging, thereby influencing the charging performance and charging time of the battery. To this end, this paper considers the influence of ambient temperature on battery charging performance, and collaboratively optimizes the number of charging piles in the bus depot and the scheduling problem of EB charging. Aiming at minimizing the cost of laying charging piles in bus stations and the charging costs of bus fleets, as well as minimizing the empty time of electric bus fleets and waiting time for charging in queues, a mixed-integer nonlinear programming model is established, and the immune algorithm is used to solve it. At last, an actual bus depot and four EB routes are taken as examples for verification. The results show that by optimizing the charging waiting time of the electric bus at the bus station, the rapid decline in charging performance caused by the sharp drop in battery temperature is avoided. Without increasing the charging cost of the electric bus fleet, the established method reduces the charging pile installation cost, improves the bus depot's service efficiency, and ensures the punctuality and integrity of the regional bus route operation.

**Keywords:** electric bus; bus depot; charging scheduling; ambient temperature; waiting time



**Citation:** Wang, J.; Wang, H.; Wang, C. Optimal Charging Pile Configuration and Charging Scheduling for Electric Bus Routes Considering the Impact of Ambient Temperature on Charging Power. *Sustainability* **2023**, *15*, 7375. <https://doi.org/10.3390/su15097375>

Academic Editor: Tamás Bányai

Received: 5 April 2023

Revised: 19 April 2023

Accepted: 22 April 2023

Published: 28 April 2023



**Copyright:** © 2023 by the authors. Licensee MDPI, Basel, Switzerland. This article is an open access article distributed under the terms and conditions of the Creative Commons Attribution (CC BY) license (<https://creativecommons.org/licenses/by/4.0/>).

## 1. Introduction

Sustainable, emission-free transportation is key to improving the quality of life in cities. The energy-saving and environmental benefits of electric buses (EBs) are increasingly recognized, leading to governments worldwide implementing policies to transition from traditional fuel-powered bus fleets to electric fleets. China has established itself as a leader in the EB market, with 419,500 pure EBs operating in Chinese cities at the end of 2021, accounting for 62.6% of the global total [1]. Global EB deployment is projected to reach 4.5 million by 2030 [2]. However, the rapid expansion of the EB scale also brings new challenges, especially regarding choosing the charging infrastructure that adheres to techno-economic constraints to support the operational needs of routes [3]. Bus depots are usually located on the property of the transit agency and have a lower up-front capital cost, not requiring negotiations or leases of property around the service area [4]. Therefore, a limited number of charging piles are usually built in one or more depots to provide charging services for regional EB routes.

However, it is common for multiple EB routes sharing the same bus depot to operate in an island mode. The scheduling and charging plans for these routes are often independent of each other, which can result in overlapping charging demands. Consequently, EBs on

certain routes may not be able to adhere to their charging plans due to charging piles being occupied by EBs from other routes, which seriously impacts the punctuality of their subsequent service trips. Additionally, EB fleets often have to wait in line for charging, limited by the number of charging piles in the bus depot. Particularly in low-temperature environments, prolonged charging waiting times could cause a decrease in the temperature and an increase in the internal resistance of the lithium-ion battery, leading to early termination of the constant current stage and transition to the constant voltage stage. This, in turn, can significantly extend battery charging time [5]. Under extreme low-temperature conditions, the battery's electrolyte may even freeze, rendering it impossible to charge. These issues can significantly impact the integrity of the follow-up service for some EB routes, resulting in interrupted service due to insufficient power. As a result, rational planning of the number of charging piles in bus depots, as well as scientific allocation of charging positions, queuing times, and charging times for the EB fleet, are essential to improving the service efficiency of EB depots, ensuring punctuality and service integrity of the route itinerary, and reducing the economic costs of bus companies.

This paper focuses on the collaborative optimization problem of charging pile configuration and EB charging schemes. Firstly, the impact of EB charging queuing time on battery temperature at the beginning of charging was quantified, taking into consideration different ambient temperatures. Additionally, the functional relationship between the charging time and charging amount is described under the influence of different battery temperatures for the common constant current and constant voltage-charging mode. Subsequently, under the scenario of known multi-route EB vehicle scheduling schemes and energy consumption demand, a mixed-integer nonlinear programming model was developed with the objectives of minimizing the deployment costs of charging piles, charging costs, deadhead time, and queuing time of the EB fleet, and an immune algorithm was used to solve it. Finally, the effectiveness of the proposed optimization method was verified through its practical application to an actual bus depot and EB routes.

The subsequent sections of this paper are arranged as follows. Section 2 gives a review of the relevant literature regarding EB charging-scheduling methods. In Section 3, we develop a mixed-integer nonlinear programming model and devise a solution algorithm to address the collaborative optimization problem of charging pile configuration and EB charging schedule. Section 4 presents a case study based on an actual bus depot and EB routes. Finally, the research conclusions and prospects for future research can be found in Section 5.

## 2. Literature Review

In order to address the limited driving range of EBs and alleviate driver anxiety, it is common practice for EBs to utilize idle time during off-peak electricity pricing periods to recharge their batteries. In this context, a well-designed charging-scheduling scheme can significantly improve the service quality of EB routes and reduce operating costs [6–9]. Existing research on charging scheduling for EB fleets can be broadly categorized into three categories: single-route EB fleet charging scheduling, multi-route EB fleet charging scheduling, and charging scheduling in depots.

In the charging-scheduling problem of a single-route EB fleet, the prevailing approach was to develop optimization models that aimed to minimize costs, such as vehicle purchase costs, charging costs, and charging pile deployment costs. For instance, He et al. [10] proposed an optimization model that leverages the rolling horizon scheduling method to solve the EB charging problem, which considers not only the costs of charging stations and batteries but also a time-of-use electricity cost rate structure. Hu et al. [11] developed an optimization model that takes the cost of extra waiting, time-varying electricity prices, and various battery capacities into account, and solved it using a genetic algorithm. Jiang et al. [12] presented a model to optimize the charging schedule with the objective of minimizing the annualized total cost (including the fixed cost of EB and charging costs) and developed a neighborhood search-based heuristic algorithm considering charging

and dispatching policies to solve it. He et al. [13] formulated the charging schedule and management optimization model of EBs into a linear program that can minimize both upfront investment and charging costs. To achieve the purpose of reducing the overall charging and operating costs for city-scale EB fleets, Wang et al. [14] considered the time-variant electricity pricing and designed an effective pricing-aware real-time charging-scheduling system using a Markov Decision Process. Liu et al. [15] indicated the nonlinear increase in energy consumption rate with the decrease in temperature and established a charging-scheduling model considering time-of-use tariff and stochastic trip travel times.

However, in reality, charging piles built in one or more depots usually need to jointly provide charging services for regional EB routes. However, when a relatively large number of buses queue up for charging, the original charging schedule may not be executed as planned, which can significantly impact the subsequent vehicle scheduling scheme [16].

In order to solve the aforementioned challenges, some scholars focused on the EB fleets of multiple routes and limited the number of EBs simultaneously charged in the bus depot, so as to optimize the charging plan of the multi-route EB fleets collaboratively. Zeng et al. [17] coordinated charging events among multi-route fleets by transferring the start time of scattered charging events, so as to realize the spatial-temporal balanced distribution of charging demands for multi-route fleets. Wang et al. [18] established a mixed-integer programming optimization model based on the technology of the fast-charging system to jointly optimize the location, capacity, and charging plan of the charging facilities in the public transportation system. Zhang et al. [19] incorporated the cost changes caused by battery degradation and the nonlinear charging curve in the charging process into the optimization framework to solve the charging-scheduling problem of multi-route buses. Fang et al. [20] studied the charging plans of the EB fleet under different charging strategies with the goal of minimizing the total construction cost in long-term operations. Ding et al. [21] jointly optimized the charge-discharge plan of the energy storage system and the charging scheme of EBs, aiming to minimize the total investment cost and charging cost of the fast-charging electric public transportation system. However, most of the existing literature has focused on optimizing the charging plan of bus fleets when the number of charging piles in the bus depot(s) is known, lacking approaches addressing the joint optimization of the bus depot capacity and the charging plan.

Charging scheduling in EB depots is another effective way to solve bus charging conflicts on multi-route bus routes. Zheng et al. [22] took the uncertainty of overnight charging time into account and designed a model with the objective of minimizing the expected total charging cost (including the in-service cost, energy consumption cost, and penalty cost due to overly low charging). Based on the night charging management method, Houbbadi et al. [23] proposed a nonlinear programming model with the goal of minimizing the cost of battery aging. Jahic et al. [24] proposed two charging-scheduling algorithms to minimize the peak load for large bus depots, aiming at the problems of unevenly distributed load profiles with high load peaks caused by multi-bus charging in the depot. Despite some research efforts focusing on the charging-scheduling problems of EB fleets during nighttime, where the start and end time of charging is relatively flexible and does not need to guarantee punctual service trip departures after charging completion, limited attention has been given to daytime charging-scheduling problems. Moreover, even in the few existing works that consider daytime charging demands, they fail to account for the effect of EB waiting times at depots on battery charging performance under different ambient temperatures. Additionally, none of these works establishes a joint optimization method for both the depot capacity and charging plan of the EB fleet.

### 3. Methodology

#### 3.1. Problem Description

Public transit bus depots are usually equipped with several charging piles to facilitate EBs docking and their replenishment during idle time. The number of regional bus depots is denoted as  $M$ . These depots jointly serve multiple EB routes. Let  $n$  be the EB route



number, where  $n = 1, 2, \dots, N$ . The locations of the departure and terminal stations of each EB route are fixed. Let  $T_{m,n}^{dep}$  represent the average deadhead time (unit: min) of the EB between depot  $m$  and the departure station of route  $n$ , and  $T_{m,n}^{term}$  represents the average deadhead time (unit: min) of the EB between depot  $m$  and the terminal station of route  $n$ , where  $m = 1, 2, \dots, M$ .

The trip chain of EBs on the route is known [25]. Let  $D_k^j$  represent the end time of the trip before the  $j$ -th charge of EB  $k$ , and  $B_k^j$  represents the start time of the trip after the  $j$ -th charge of EB  $k$ , where  $k = 1, 2, \dots, K$ ,  $j = 1, 2, \dots, J_k$ .  $K$  denotes the EB fleet size;  $J_k$  is the maximum possible charging times for EB  $k$ . Let the location state of EB  $k$  at time  $D_k^j$  be  $S_{k,n}^j \in \{0, 1\}$ . If  $S_{k,n}^j = 1$ , and EB  $k$  is at the departure station of route  $n$ , otherwise EB  $k$  is at the terminal station of route  $n$ . Similarly, let the location state of EB  $k$  at time  $B_k^j$  be  $\tilde{S}_{k,n}^j \in \{0, 1\}$ . If  $\tilde{S}_{k,n}^j = 1$ , EB  $k$  is at the departure station of route  $n$ , otherwise it is at the terminal station of route  $n$ . Moreover, the energy consumption on the bus route of the EB between the  $j$ -th charging task and the  $j + 1$ -th charging task (excluding the deadhead energy consumption of the EB between the depot and the departure/terminal stations) is expressed as  $W_k^{j,j+1}$ , with the unit being kWh. In particular,  $W_k^{0,1}$  is the energy consumption on the bus route of EB  $k$  from the start of operation to the start of the first charging task, and  $W_k^{J,J+1}$  is the energy consumption on the bus route of EB  $k$  from the end of the last charging task  $J$  to the end of operation.

We define a binary decision variable  $x_{k,m}^j \in \{0, 1\}$  to indicate whether EB  $k$  completes the  $j$ -th charging task at the bus depot  $m$ . If  $x_{k,m}^j = 1$ , EB  $k$  charges at the bus depot  $m$ , otherwise it does not. Let the integer decision variable  $\hat{T}_{k,m}^j$  be the queuing time (unit: s) of EB  $k$  after arriving at the bus depot  $m$  and before the  $j$ -th charging, and  $T_{k,m}^j$  represents the  $j$ -th charging time of EB  $k$  at the bus depot  $m$  (unit: s). Apart from that, the integer decision variable  $U_m$  denotes the capacity of bus depot  $m$ , which represents the maximum number of EBs that can be charged simultaneously in the bus depot  $m$ .

### 3.2. Charging Time Settings

To prevent the potential destruction of battery structure and subsequent battery failure and explosion due to the internal polarization resulting from continuous battery voltage increase, the constant current constant voltage (CC-CV) charging method is typically employed [26]. During the CC stage, the charging current remains constant, resulting in a linear increase in the battery's SOC over time. During the CV stage, the battery terminal voltage remains constant, and the current decreases exponentially, causing the battery SOC to increase nonlinearly with a convex shape over time. The relationship between the SOC of EBs and the charging time is complex and non-linear. In order to simplify the model, most existing research utilizes a piecewise function to approximate the charging power and sets the 80% SOC level as the turning point between the CC stage and the CV stage [19,27,28].

Actually, the charging performance of lithium-ion batteries can be influenced by both the external ambient temperature and the internal temperature of the battery. Several studies have demonstrated that, in comparison to room temperature environments, low-temperature conditions cause the batteries to enter the CV phase earlier during the charging process and prolong the overall charging time [29,30]. When  $x_{k,m}^j = 1$ , we take a random charging task of EB  $k$  in an outdoor low-temperature environment as an example, as shown in Figure 1. In interval  $[D_k^j, t_1]$ , when the EB returns to the depot without passengers, the battery experiences discharge, leading to a rapid increase in temperature that exceeds the ambient temperature; in interval  $[t_1, t_2]$ , when EBs are queued up at the depot, there exists a temperature difference between the battery temperature and the ambient temperature, resulting in heat transfer, causing the battery temperature to gradually decrease; in interval  $[t_2, t_4]$ , the battery undergoes CC-CV charging, generating only a small amount of heat through internal chemical reactions, resulting in a slow rise in battery temperature. In

interval  $[t_4, B_k^j]$ , battery charging is finished and waiting for the next service trip, resulting in the battery temperature gradually cooling to the ambient temperature.

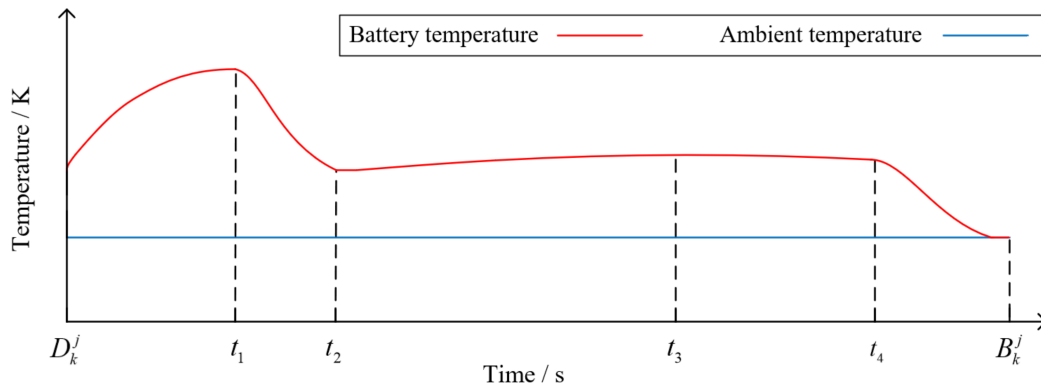


**Figure 1.** Illustration of electric bus battery temperature changing with time and ambient temperature.

The battery temperature of EB  $k$  when it arrives at the bus depot for the  $j$ -th charging task is recorded as  $H_k^j(t_1)$  (unit: K), where  $t_1 = D_k^j + S_{k,n}^j \times T_{m,n}^{dep} + (1 - S_{k,n}^j) \times T_{m,n}^{term}$ . When  $H_k^j(t_1)$  is higher than the ambient temperature  $H_0$  (unit: K), the heat is transferred from the battery to the environment, and the battery gradually cools naturally. Based on Newton's cooling law [31], the calculation method of the battery temperature  $H_k^j(t_2)$  of EB  $k$  at the start of the  $j$ -th charging is shown in Equation (1), where  $t_2 = t_1 + \hat{T}_{k,m}^j$ .

$$H_k^j(t_2) = (H_k^j(t_1) - H_0)e^{-\lambda \hat{T}_{k,m}^j} + H_0, \quad (1)$$

where  $\lambda$  is a positive constant;  $\lambda = hA/C$ , where  $h$  is the heat transfer coefficient of the air-battery interface,  $\text{W} \cdot \text{m}^{-2} \cdot \text{K}^{-1}$  [32];  $A$  is the battery surface area,  $\text{m}^2$ ; and  $C$  is the battery heat capacity,  $\text{J/K}$ .

In the CC charging stage, based on the law of battery energy conservation, the following Equation (2) holds true:

$$\theta \omega \frac{(H_k^j(t_3) - H_k^j(t_2))}{t_3 - t_2} = \int_{t_2}^{t_3} \left( I^2 R_k(t) + I H_k^j(t) \times \frac{dU_k^{ov}}{dH_k^j} \right) dt - hA (H_k^j(t_3) - H_k^j(t_2)), \quad (2)$$

where  $t_3$  denotes the end time of CC charging stage;  $H_k^j(t_3)$  is the battery temperature at  $t_3$  of EB  $k$ , K;  $\theta$  is the heat capacity of the battery units,  $\text{J} \cdot \text{kg}^{-1} \cdot \text{K}^{-1}$  [32];  $\omega$  represents battery mass, kg;  $I$  is the charging current in the CC charging stage, A;  $R_k(t)$  is the battery internal resistance of EB  $k$  at time  $t$ ,  $\Omega$ ; and  $dU_k^{ov}/dH_k^j$  is the entropic coefficient,  $\text{V/K}$ .

In the CV charging stage, also based on the law of battery energy conservation, the following Equation (3) holds true:

$$\theta \omega \frac{(H_k^j(t_4) - H_k^j(t_3))}{t_4 - t_3} = \int_{t_3}^{t_4} \left( \frac{(U_k^{tm})^2}{R_k(t)} + \frac{U_k^{tm} H_k^j(t)}{R_k(t)} \times \frac{dU_k^{ov}}{dH_k^j} \right) dt - hA (H_k^j(t_4) - H_k^j(t_3)), \quad (3)$$

where  $U_k^{tm}$  is the charging voltage in the CV charging stage, V;  $t_4$  is the end time of CV charging stage; and  $H_k^j(t_4)$  denotes the battery temperature at time  $t_4$ , K.

EBs need to drive to depots for charging between scheduled adjacent trip tasks. Due to the limited number of charging piles in the depot, there may be EBs waiting in line, which makes the available charging time of EBs limited. In addition, the electricity price during the day is generally higher than that at night. On the premise of avoiding the interruption of the service trip due to the exhaustion of the vehicle, reducing the charging time of the

EB fleet during the day will help save the charging cost [33]. Therefore, EBs may not necessarily be charged to the upper limit each time they are charged, or even go through two stages of CC and CV voltage. Therefore, the relationship between the charging amount  $w_{k,m}^j$  and  $T_{k,m}^j$  of the  $j$ -th charging task of EB  $k$  at the bus depot  $m$  is shown in Equation (4),

$$w_{k,m}^j = \begin{cases} \frac{x_{k,m}^j}{3.6 \times 10^6} \times \left( \int_{t_2}^{t_k^j} I^2 R_k(t) dt \right) & t_k^j \leq t_3 \\ \frac{x_{k,m}^j}{3.6 \times 10^6} \times \left( \int_{t_2}^{t_3} I^2 R_k(t) dt + \int_{t_3}^{t_k^j} \frac{(U_k^{\text{tm}})^2}{R_k(t)} dt \right) & t_3 < t_k^j \leq t_4 \end{cases}, \quad (4)$$

where  $t_k^j$  is the time when EB  $k$  finishes the  $j$ -th charging task,  $t_k^j = t_2 + T_{k,m}^j$ .

### 3.3. Model Formulation

To optimize the charging-pile configuration, and to allocate charging positions, waiting time, and charging time of the EBs in a scientific manner, we aim to minimize the deployment costs of charging piles and the charging costs of the EB fleet (Equation (5)), while considering the minimization of deadhead time and queue-waiting time of the EBs as optimization objectives (Equation (6)). The following optimization model is established:

$$\min z_1 = \sum_{m=1}^M C_m U_m + \sum_{m=1}^M \sum_{k=1}^K \sum_{j=1}^{J_k} c_m^j w_{k,m}^j, \quad (5)$$

$$\min z_2 = \sum_{m=1}^M \sum_{k=1}^K \sum_{j=1}^{J_k} \sum_{n=1}^N x_{k,m}^j \left( (S_{k,n}^j + \tilde{S}_{k,n}^j) \times T_{m,n}^{\text{dep}} + ((1 - S_{k,n}^j) + (1 - \tilde{S}_{k,n}^j)) \times T_{m,n}^{\text{term}} \right) + \sum_{m=1}^M \sum_{k=1}^K \sum_{j=1}^{J_k} x_{k,m}^j \hat{T}_{k,m}^j, \quad (6)$$

$$\text{s.t. } \sum_{m=1}^M x_{k,m}^j \leq 1 \forall k, j, \quad (7)$$

$$D_k^j + x_{k,m}^j \left( (S_{k,n}^j + \tilde{S}_{k,n}^j) \times T_{m,n}^{\text{dep}} + ((1 - S_{k,n}^j) + (1 - \tilde{S}_{k,n}^j)) \times T_{m,n}^{\text{term}} + \hat{T}_{k,m}^j + T_{k,m}^j \right) \leq B_k^j \quad \forall k, m, j, \quad (8)$$

$$W_k^{\text{avl}} + \sum_{j'=1}^j \sum_{m=1}^M w_{k,m}^{j'} - \sum_{j'=0}^j W_k^{j',j'+1} \geq W_k^{\text{min}} \quad \forall k, j, \quad (9)$$

$$W_k^{\text{avl}} + \sum_{j'=1}^j \sum_{m=1}^M w_{k,m}^{j'} - \sum_{j'=0}^{j-1} W_k^{j',j'+1} \leq W_k^{\text{max}} \quad \forall k, j, \quad (10)$$

$$\sum_{k=1}^K \gamma_{k,m}(t) \leq U_m \quad \forall m, t, \quad (11)$$

$$U_m \leq \tilde{U}_m \quad \forall m, \quad (12)$$

$$T_{k,m}^j \geq T_k^{\text{min}} \quad \forall k, j, m, \quad (13)$$

$$S_{k,n}^j \in \{0, 1\} \quad \forall k, j, n, \quad (14)$$

$$\hat{T}_{k,m}^j, T_{k,m}^j, U_m \in \mathbb{N} \quad \forall k, j, m, \quad (15)$$

where  $C_m$  is the daily average cost of each charging pile deployed in the bus depot  $m$ , CNY/pile.  $c_m^j$  is the electricity price of the charging task  $j$  of the bus in the bus depot  $m$ , CNY/kWh.  $W_k^{\text{avl}}$  is the available battery power of EB  $k$  when it starts to operate every day,

kWh.  $W_k^{\min}$  and  $W_k^{\max}$  are, respectively, the lower and upper limits of the battery power of EB  $k$ , kWh. When  $x_{k,m}^j = 1$ , let  $\gamma_{k,m}(t) \in \{0, 1\}$  denote the charging state of EB  $k$  at time  $t$  within depot  $m$ . If  $\gamma_{k,m}(t) = 1$ , the EB is charging; otherwise not.  $\tilde{U}_m$  represents the maximum number of charging piles allowed to be installed in the depot  $m$ .  $T_k^{\min}$  is the minimum charging time of EB  $k$ , s.

Constraint (7) stipulates that each charging task of EBs can only be completed in one depot. Constraint (8) requires that each charging task of an EB should be time-feasible to ensure that the next trip departs on time. Constraint (9) restricts that the remaining battery power of the EB should be greater than or equal to  $W_k^{\min}$  before the start of each charging task, so to prevent the battery from being over-discharged and damaged. Constraint (10) constrains that the battery power of the EB should be less than or equal to  $W_k^{\max}$  after each charging task, so as to avoid potential safety hazards caused by battery overcharging. Constraint (11) ensures that the number of EBs charging simultaneously in each bus depot cannot exceed the capacity of the depot. Due to the limited land area of the bus depot, the number of charging piles at each depot must not exceed  $\tilde{U}_m$ , as shown in constraint (12). In order to avoid frequent battery charging, constraint (13) stipulates that the charging time of each EB should be greater than or equal to  $T_k^{\min}$ . Constraints (14) and (15) give the value ranges of optimization variables.

### 3.4. Solution Algorithm

The mixed-integer nonlinear programming model proposed in this study for collaborative optimization of charging-pile configuration and multi-route EB charging-scheduling scheme is a challenging NP-hard problem that involves a large number of 0–1 variables and integer variables. Section 3.2 of this study takes into account the impact of parameter  $\hat{T}_{k,m}^j$  on battery temperature and parameter  $T_{k,m}^j$ . Equation (4) reveals that the indirect variable  $w_{k,m}^j$  is not only a nonlinear function of optimization variables  $\hat{T}_{k,m}^j$  and  $T_{k,m}^j$ , but also involves the product of binary variable  $x_{k,m}^j$  and integer variable  $T_{k,m}^j$ , making linearization difficult and the exact optimization methods challenging to apply.

Artificial intelligence optimization algorithms offer unique advantages for solving problems that involve multiple variables, nonlinearity, discontinuity, and multiple constraints. However, certain algorithms encounter challenges such as slow convergence speed and a tendency to fall into local optima. In contrast, the Immune Algorithm (IA) is an intelligent optimization algorithm that has been artificially designed by mimicking biological immune mechanisms and incorporating genetic evolution mechanisms. This algorithm possesses the benefits of adaptability, randomness, parallelism, global convergence, and population diversity (as highlighted in the work of reference [34]). Unlike other optimization algorithms, the IA maintains population diversity and overcomes local convergence problems by leveraging its unique characteristics, ultimately enabling the attainment of globally optimal solutions [35].

Combined with practical problems, the key steps of the IA are designed as follows:

Step 1: Let the number of iterations  $g = 0$  and carry out antigen recognition and antibody coding. The antigen refers to the mathematical model of the problem being solved, comprising optimization objectives and constraints as presented in Equations (5) to (15). The effectiveness of the operator is directly dependent on the rationality of antibody coding. Hence, a parallel integer coding approach is employed, whereby the immune cell antibody consists of  $K$  gene fragments, each with a length of  $Y = 3 \times \max_{k=1,2,\dots,K} (J_k)$ , as depicted in Figure 2.

$k=1$	$m$	$m$	$\hat{T}_{1,m}^1$	$\hat{T}_{1,m}^2$	$T_{1,m}^1$	$T_{1,m}^2$	0	0	0	$J_k = 2$
$k=2$	$m$	$m$	$m$	$\hat{T}_{2,m}^1$	$\hat{T}_{2,m}^2$	$\hat{T}_{2,m}^3$	$T_{2,m}^1$	$T_{2,m}^2$	$T_{2,m}^3$	$J_k = 3$
...										...
$k=K$	$m$	$m$	$m$	$\hat{T}_{K,m}^1$	$\hat{T}_{K,m}^2$	$\hat{T}_{K,m}^3$	$T_{K,m}^1$	$T_{K,m}^2$	$T_{K,m}^3$	$J_k = 3$

**Figure 2.** Illustration of immune antibody coding.

Step 2: Population initialization. The original population is generated randomly. It should be noted that the gene node must be a valid node to join the initial population, which satisfies the constraints (7) to (15). Set the initial population size to  $E$ .

Step 3: Determine whether  $g \geq G$ , where  $G$  is the set maximum number of iterations. If not, proceed to Step 4, otherwise the algorithm terminates.

Step 4: Calculate the affinity between antigen and antibody. Since there are two optimization objectives in this paper, both of which are minimum value problems, we use Equation (16) to calculate the affinity  $Z(a)$  between any antibody  $a$  and antigen.

$$Z(a) = -(\alpha_1 z_1(a) + \alpha_2 z_2(a)), \quad (16)$$

where  $z_1(a)$  and  $z_2(a)$  represent the value of the first objective function (as shown in Equation (5)) and the value of the second objective function (as shown in Equation (6)) of antibody  $a$ , respectively.  $\alpha_1$  and  $\alpha_2$  are weight parameters for the optimization objective.

Step 5: Generate immune memory cells. Store the  $Q$  antibodies with the highest affinity in the current population into the memory population.

Step 6: Assess the concentration of the population antibodies, which is employed to gauge the diversity of the antibody population. When the antibody concentration is excessive, it implies that a vast number of individuals within the population are highly similar, thereby hindering global optimization. The concentration  $\text{den}(a)$  of any antibody  $a$  can be computed using Equations (17) and (18).

$$\text{den}(a) = \frac{1}{E} \sum_{a=1}^E O(a, b), \quad (17)$$

$$O(a, b) = \begin{cases} 1 & \text{if } \sqrt{\sum_{k=1}^K \sum_{i=1}^Y (a_{k,y} - b_{k,y})^2} < \delta_o \\ 0 & \text{if } \sqrt{\sum_{k=1}^K \sum_{i=1}^Y (a_{k,y} - b_{k,y})^2} \geq \delta_o \end{cases}, \quad (18)$$

where  $O(a, b)$  denotes the similarity between antibody  $a$  and antibody  $b$ ;  $a_{k,y}$  and  $b_{k,y}$  are, respectively, the values of the  $y$ -th fragment of the  $k$ -th dimension gene of antibody  $a$  and antibody  $b$ ;  $y = 1, 2, \dots, Y$ ;  $\delta_o$  is the similarity threshold.

Step 7: Compute the degree of antibody stimulation. The degree of stimulation of an antibody indicates its quality and it is determined based on a combination of antibody affinity and concentration. Typically, antibodies with high affinity and low concentration receive greater stimulation degrees. Equation (19) illustrates the method for computing the stimulation degree  $\text{sim}(a)$  of any given antibody  $a$ .

$$\text{sim}(a) = Z(a) \cdot e^{-\beta \text{den}(a)}, \quad (19)$$

where  $\beta$  is the computing parameter, which can be determined according to practical circumstances.

Step 8: Conduct an immune operation on the antibody population by selecting the antibodies with the top- $\eta$  (unit: %) stimulation degrees and conducting cloning operations

on them by replicating each of them  $F$  times. Next, the cloned antibodies undergo mutation via the mutation operator to introduce affinity mutations and facilitate local searches. When dealing with integer-encoded antibodies, the mutation operator can be represented by Equation (20):

$$\text{vat}(a_{k,y}^f) = \begin{cases} a_{k,y}^f + (\text{rand} - 0.5) \cdot \varepsilon_{k,y} & \text{if rand} < p_0 \\ a_{k,y}^f & \text{others} \end{cases}, \quad (20)$$

where  $a_{k,y}^f$  is the value of the  $y$ -th fragment of the  $k$ -th dimension gene for the  $f$ -th clone of antibody  $a$ ,  $f = 1, 2, \dots, F$ ; rand is a function used to generate random numbers in the range 0 to 1;  $\varepsilon$  is the defined neighborhood range; and  $p_0$  is the mutation probability.

Step 9: The population refreshes. In this stage, antibodies failing to satisfy the constraints (7) to (15) after mutation are removed. If the population size still exceeds  $E$ , antibodies with lower stimulation degrees are also eliminated. In case the population size is less than  $E$ , a feasible solution is randomly generated and included to form a new generation of antibodies. Next,  $Q$  antibodies with the highest affinity in the current iteration process are chosen, compared, and replaced with those in the memory population. Finally, the memory population is updated, and  $g = g + 1$  to proceed to Step 3.

## 4. Case Study

### 4.1. Data Investigation

This study utilizes a depot and four EB routes in a specific Chinese city as a case study and gathers operational data from 3 January 2023, to verify and analyze the proposed optimization approach. The average ambient temperature during the data collection period was  $-16^\circ\text{C}$ , equivalent to 257.15 K. The departure station (DS) for Routes I, II, and III is located in the depot, which has nine charging piles. There is a deadhead time between both the departure and terminal stations and the depot for Route IV, as depicted in Figure 3.

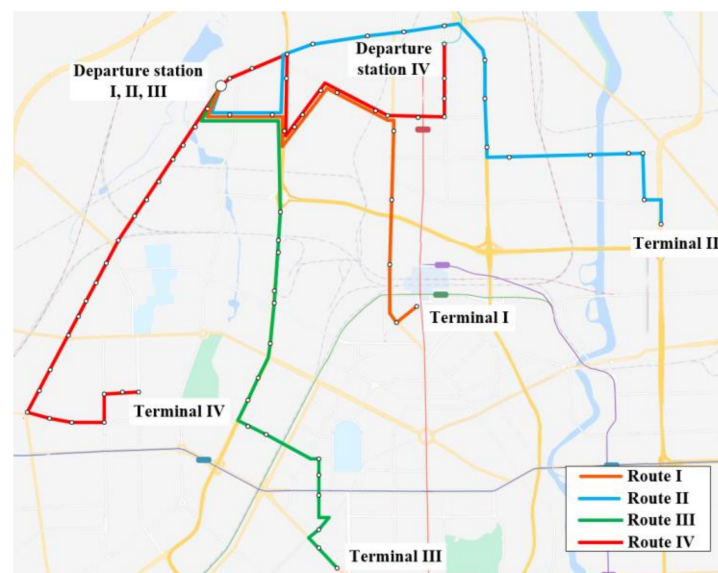


**Figure 3.** Sketch diagram of four electric bus routes.

The city implements a time-of-use electricity pricing policy, which has six time periods throughout the day and three pricing tiers, namely peak, shoulder, and off-peak prices, as presented in Table 1.



**Table 1.** Time-of-use electricity price schedule.

Index	Period	Electricity Price (CNY/kWh)	Index	Period	Electricity Price (CNY/kWh)
1	5:00–7:30	1.0866	2	7:30–11:00	1.3574
3	11:00–15:30	1.0866	4	15:30–21:00	1.3574
5	21:00–22:00	1.0866	6	22:00–5:00	0.8158

Table 2 presents the fundamental characteristics of the four EB routes, which use the lithium iron phosphate batteries with a rated capacity of 162 kWh. The EBs on Route I and Route II were acquired in November 2020, whereas those on Route III and Route IV were procured in March 2022, resulting in differences in the state of health (SOH) among the vehicles serving different routes. Based on the historical charging data, the estimated SOH for vehicles on Route I, Route II, Route III, and Route IV are 95.5%, 95.5%, 98%, and 97%, respectively.

**Table 2.** Basic information of routes.

Route	Route I	Route II	Route III	Route IV
Number of vehicles	31	22	25	25
Uplink DS (downlink terminal)	DS I	DS II	DS III	DS IV
Uplink terminal (downlink DS)	Terminal I	Terminal II	Terminal III	Terminal IV
Operating hours of DS	4:50–21:30	5:30–19:00	5:30–20:00	5:20–18:30
Operating hours of terminal	5:20–22:00	6:10–19:35	6:10–20:50	5:30–19:10
Departure headway (min)	3–10	5–10	5–6	6–7
Route mileage (km)	9.4	13.2	11.6	16.8
Number of uplink trips	233	129	162	128
Number of downlink trips	233	129	162	133
$T_{m,n}^{term}$ (min)	–	–	–	15
$T_{m,n}^{dep}$ (min)	0	0	0	17
One-way average energy consumption (kWh)	6.4	7.9	7.5	11.5

The EBs on the four routes have been numbered for convenience. Specifically, vehicles numbered 1–31 correspond to Route I, vehicles numbered 32–53 correspond to Route II, vehicles numbered 54–78 correspond to Route III, and vehicles numbered 79–103 correspond to Route IV. The numbers of service trips and total operating mileage of each EB on a given route are different. Some EBs can operate all day without requiring a charging task, as their maximum available battery power is sufficient to meet their needs. During the day, approximately 43.7% of the EBs in the bus network require charging, and these tasks are concentrated in the shoulder electricity price period. Table 3 presents the available charging time windows on the multi-route EBs' trip chain, along with their arrival and departure locations on the route before and after charging.

To ensure the performance and longevity of the battery system, the EB battery thermal management system operates within a suitable temperature range [36]. In this study, the battery temperature of EB  $k$  is set to 298.15 K when it arrives at the bus depot for the  $j$ -th charging task. Previous research has shown that the internal resistance does not significantly change when the battery operates within the range of 293–323 K [37]. Thus, if the EB returns to the depot and can be charged immediately, the charging power during the CC stage can be regarded as approximately equal to the nominal value of 100 kW. Additionally,  $dU_k^{ov}(t)/dH_k^j(t)$  is related to the electrochemical reaction, which is usually considered a constant and set as 0.3 mV·K<sup>−1</sup> [38].

**Table 3.** Charging tasks of EB fleets.

Route No.	EB No.	$J_k$	$[D_k^j, B_k^j]$	Arrival Location	Departure Location
Route I	1	3	[5:52, 6:30] [11:03, 14:05] [15:16, 15:39]	DS I	DS I
Route I	2	3	[6:02, 6:36] [11:11, 14:15] [15:26, 15:45]	DS I	DS I
Route I	3	2	[6:12, 6:42] [11:19, 14:30]	DS I	DS I
Route I	4	2	[6:22, 6:48] [11:27, 14:45]	DS I	DS I
Route I	5	2	[6:27, 6:54] [11:35, 15:00]	DS I	DS I
Route I	6	2	[6:38, 7:00] [11:43, 15:06]	DS I	DS I
Route I	7	2	[6:46, 7:06] [11:51, 15:18]	DS I	DS I
Route I	8	2	[6:51, 7:12] [11:59, 15:30]	DS I	DS I
Route III	54	3	[6:50, 7:50] [11:38, 12:30] [14:00, 14:35]	DS III	DS III
Route III	55	3	[6:56, 7:55] [11:44, 12:35] [14:05, 14:40]	DS III	DS III
Route III	56	3	[7:02, 8:00] [11:50, 12:40] [14:10, 14:45]	DS III	DS III
Route III	57	3	[7:08, 8:06] [11:56, 12:45] [14:15, 14:50]	DS III	DS III
Route III	58	3	[7:14, 8:12] [12:02, 12:50] [14:20, 14:55]	DS III	DS III
Route III	59	3	[7:20, 8:18] [12:08, 12:55] [14:25, 15:00]	DS III	DS III
Route III	60	3	[7:26, 8:24] [12:14, 13:00] [14:30, 15:06]	DS III	DS III
Route III	61	2	[12:30, 13:05] [14:35, 15:12]	DS III	DS III
Route III	62	2	[12:35, 13:10] [14:40, 15:18]	DS III	DS III
Route III	63	2	[12:40, 13:15] [14:45, 15:24]	DS III	DS III
Route III	64	2	[12:45, 13:20] [14:50, 15:30]	DS III	DS III
Route III	65	2	[12:50, 13:25] [14:55, 15:36]	DS III	DS III
Route IV	79	3	[6:20, 7:02] [11:20, 12:14] [14:02, 15:00]	DS IV	DS IV
Route IV	80	3	[6:26, 7:08] [11:26, 12:21] [14:09, 15:06]	DS IV	DS IV
Route IV	81	3	[6:32, 7:14] [11:32, 12:28] [14:16, 15:12]	DS IV	DS IV
Route IV	82	3	[6:38, 7:20] [11:38, 12:35] [14:23, 15:18]	DS IV	DS IV
Route IV	83	3	[6:44, 7:26] [11:44, 12:42] [14:30, 15:24]	DS IV	DS IV
Route IV	84	3	[6:50, 7:32] [11:50, 12:49] [14:37, 15:30]	DS IV	DS IV
Route IV	85	3	[6:56, 7:38] [11:56, 12:56] [14:44, 15:36]	DS IV	DS IV
Route IV	86	3	[7:02, 7:44] [12:02, 13:03] [14:51, 15:42]	DS IV	DS IV
Route IV	87	3	[7:08, 7:50] [12:08, 13:10] [14:58, 15:48]	DS IV	DS IV
Route IV	88	2	[12:14, 13:17] [15:05, 15:54]	DS IV	DS IV
Route IV	89	2	[12:20, 13:24] [15:12, 16:00]	DS IV	DS IV
Route IV	90	1	[12:26, 13:31]	DS IV	DS IV
Route IV	91	1	[12:32, 13:38]	DS IV	DS IV
Route IV	92	1	[12:38, 13:45]	DS IV	DS IV
Route IV	93	1	[12:45, 13:52]	DS IV	DS IV
Route IV	94	1	[12:52, 13:59]	DS IV	DS IV
Route IV	95	1	[12:59, 14:05]	DS IV	DS IV
Route IV	96	1	[13:06, 14:11]	DS IV	DS IV
Route IV	97	1	[13:13, 14:17]	DS IV	DS IV
Route IV	98	1	[13:20, 14:23]	DS IV	DS IV
Route IV	99	1	[13:27, 14:29]	DS IV	DS IV
Route IV	100	1	[13:34, 14:35]	DS IV	DS IV
Route IV	101	1	[13:41, 14:41]	DS IV	DS IV
Route IV	102	1	[13:48, 14:47]	DS IV	DS IV
Route IV	103	1	[13:55, 14:53]	DS IV	DS IV

The other essential input parameters in the model are shown in Table 4. Among them, the daily average deployment cost of the charging pile is obtained by dividing the deployment cost of the charging pile by the service life. The deployment cost of each charging pile is 100,000 CNY/pile, and the service life is 10 years.

**Table 4.** Values of input parameters in the model.

Parameters	Values	Parameters	Values
$C_m$	27.4 CNY/pile	$A$	2.06 m <sup>2</sup>
$W_k^{\max}$	145.8 kWh	$h$	11 W·m <sup>-2</sup> ·K <sup>-1</sup>
$W_k^{\min}$	48.6 kWh	$\theta$	1006.43 J·kg <sup>-1</sup> ·K <sup>-1</sup>
$T_k^{\min}$	10 min	$\omega$	183.0 kg
$U_m$	9	$\lambda$	0.0012

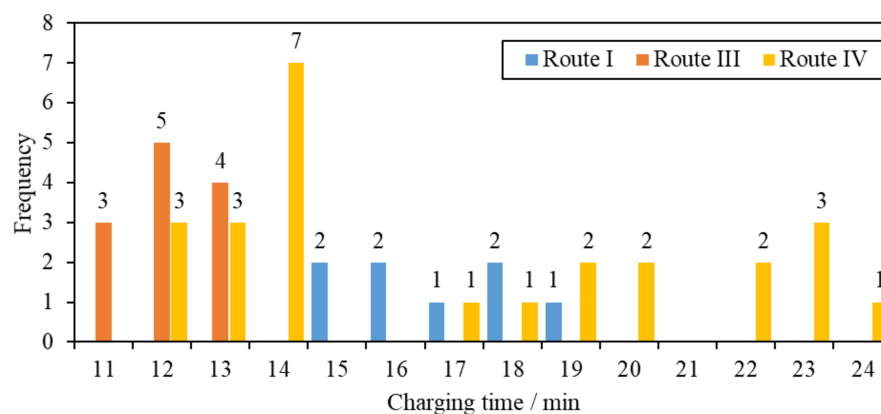
#### 4.2. Optimization Results

The model proposed in this paper was solved using Python 3.8 on a computer with a 2.90 GHz CPU and 16GB RAM. The weight coefficients were  $\alpha_1 = 0.3$  and  $\alpha_2 = 0.7$ . The initial population size  $E$ , the maximum number of iterations  $G$ , the mutation probability  $p_0$ , and the similarity threshold  $\delta_0$  were set to 50, 200, 0.01, and 0.7, respectively. The algorithm was able to find the optimal solution within 460 s.

The optimized number of charging piles in the depot was 5, and the daily charging cost of the EB fleet  $z_1$ , and the empty driving time of the fleet  $z_2$ , were 1432.2 CNY and 375 min, respectively. Among them, the average daily deployment cost of charging piles was found to be 137 CNY, and the cost of charging the EB fleet was 1295.2 CNY. The EB fleet deadhead time was 375 min (all generated by the EBs of Route IV) and the EB queuing waiting time was 0 min. The average daily deployment cost of charging piles was found to be 137 CNY, and the charging plan generated by the algorithm is presented in Table 5.

The optimization approach proposed in this study has led to a reduction of 4 charging piles in the depot, resulting in cost savings of 400,000 CNY for charging pile deployment compared to the current setup. This paper also addresses the impact of temperature on battery-charging power in the EB charging-scheduling problem, carefully manages the queuing time of EBs at bus depots, and mitigates the risk of a rapid decline in charging performance caused by a sharp drop in battery temperature. Consequently, it has enhanced the operational efficiency of the bus depot without increasing the charging cost of the EB fleet, and has ensured the punctuality and integrity of the regional bus routes.

Figure 4 depicts the charging-time distribution of the EB fleet, demonstrating that all EBs can complete their charging task within 30 min. This can be attributed to the fact that, under the background of time-of-use electricity price, the price of charging electricity at night is low, so the EB fleet only needs to replenish enough electricity to complete the operation tasks of the day during the day. Additionally, the total charging time is influenced more significantly by the average charging power during the CV stage than the CC stage. To address this issue, the proposed optimization solution enables the EBs to undergo a rapid recharge with a constant power of approximately 100 kW during the CC stage without transitioning to the CV stage.

**Figure 4.** Charging time distribution of electric bus fleet.

**Table 5.** Charging plans for electric bus fleets.

Route No.	EB No.	$\hat{T}_{k,m}^j$ (min)	$[t_2, t_k^j]$	$T_{k,m}^j$ (min)	$w_{k,m}^j$ (kWh)
Route I	1	0	[11:03, 11:19]	16	25.374
Route I	2	0	[11:11, 11:27]	16	26.374
Route I	3	0	[11:19, 11:38]	19	31.374
Route I	4	0	[11:27, 11:44]	17	27.374
Route I	5	0	[11:35, 11:53]	18	29.374
Route I	6	0	[11:43, 11:58]	15	23.374
Route I	7	0	[11:51, 12:09]	18	29.374
Route I	8	0	[11:59, 12:14]	15	23.374
Route III	54	0	[11:38, 11:50]	12	19.344
Route III	55	0	[14:05, 14:16]	11	17.344
Route III	56	0	[14:10, 14:22]	12	18.344
Route III	57	0	[11:56, 12:08]	12	19.344
Route III	58	0	[14:20, 14:33]	13	21.344
Route III	59	0	[14:25, 14:38]	13	21.344
Route III	60	0	[12:14, 12:27]	13	20.344
Route III	61	0	[14:35, 14:46]	11	17.344
Route III	62	0	[12:35, 12:46]	11	17.344
Route III	63	0	[12:40, 12:52]	12	18.344
Route III	64	0	[14:50, 15:03]	13	21.344
Route III	65	0	[14:55, 15:07]	12	18.344
Route IV	79	0	[11:35, 11:58]	23	38.216
Route IV	80	0	[14:24, 14:46]	22	35.216
Route IV	81	0	[14:31, 14:51]	20	33.216
Route IV	82	0	[14:38, 15:00]	22	36.216
Route IV	83	0	[14:45, 15:05]	20	33.216
Route IV	84	0	[12:05, 12:28]	23	38.216
Route IV	85	0	[12:11, 12:34]	23	37.216
Route IV	86	0	[15:06, 15:25]	19	31.216
Route IV	87	0	[12:23, 12:40]	19	30.716
Route IV	88	0	[12:29, 12:53]	24	39.216
Route IV	89	0	[12:35, 12:52]	17	28.216
Route IV	90	0	[12:41, 12:59]	18	28.716
Route IV	91	0	[12:47, 13:00]	13	24.716
Route IV	92	0	[12:53, 13:07]	14	26.716
Route IV	93	0	[13:00, 13:14]	14	26.716
Route IV	94	0	[13:07, 13:19]	12	23.716
Route IV	95	0	[13:14, 13:26]	12	23.716
Route IV	96	0	[13:21, 13:34]	13	25.716
Route IV	97	0	[13:28, 13:42]	14	26.716
Route IV	98	0	[13:35, 13:48]	13	24.716
Route IV	99	0	[13:42, 13:56]	14	27.716
Route IV	100	0	[13:49, 14:03]	14	27.716
Route IV	101	0	[13:56, 14:10]	14	27.716
Route IV	102	0	[14:03, 14:17]	14	26.716
Route IV	103	0	[14:10, 14:22]	12	23.716

Furthermore, the charging time of EBs varies across different routes due to the varying operating distances and frequencies. Specifically, on Route I, the charging time of EBs is concentrated within the range of 15 to 19 min, while on Route III, it is concentrated within the range of 11 to 13 min. On Route IV, however, the charging time span is larger, ranging from 12 to 24 min. This is because the number of daily trips for the EBs on Route IV differs, and 44% of the buses require an additional trip. Additionally, random fluctuations in travel time and average passenger capacity between stations of different buses on the same route cause their daily energy consumption demand to fluctuate randomly, leading to variations in their charging time within a certain range.

Upon comparing Tables 3 and 5, it can be observed that the EB fleet can charge during the two shoulder periods of 5:00–7:30 and 11:00–15:30 when electricity prices are low. However, the optimized charging plan concentrates only on the period of 11:00–15:30. The reason is that during the period from 5:00 to 7:30, the EB fleet has just begun operating and there is still sufficient battery power remaining between trip chains. Therefore, even if some EB batteries are fully charged, they do not meet the minimum charging time limit as per constraint (13). Furthermore, the remaining EBs that satisfy the constraint (13) and can be charged during 5:00–7:30 are not charged enough to ensure the integrity of the full-day operation, and hence need to be replenished during 11:00–15:30. The optimized charging plan presented in this paper results in fewer charging times as compared to multiple frequent charges in a day, with the battery SOC at the beginning and end of charging closer to 50%. This will help in prolonging the service life of the battery [39].

Figure 5 shows the charging pile utilization during the shoulder electricity price period. The results demonstrate that in the time windows divided by 10 min, 74.1% of them indicate the usage of three or more charging piles, whereas 22.2% indicate the utilization of all five charging piles. The charging pile utilization rate is relatively high from 11:00 to 15:30. However, during the remaining time, the utilization rate is considerably low, and most of the charging piles remain unused. If the charging piles during their idle period are shared with social electric cars, it can not only improve the utilization rate of charging piles and increase the income of the bus companies, but also provide charging opportunities for social electric vehicles, and alleviate the shortage of social electric vehicle charging facilities.

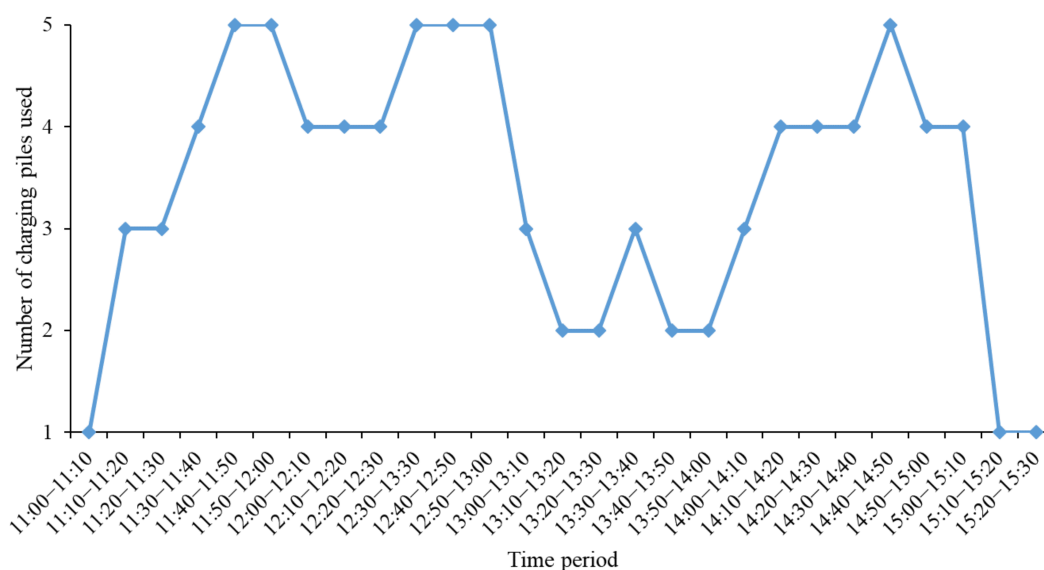


**Figure 5.** Utilization of charging piles during the shoulder electricity price period.

## 5. Conclusions

Considering the impact of queuing time on battery charging performance under different ambient temperatures, this study established a mixed-integer nonlinear programming model to collaboratively optimize the charging pile configuration, and the charging location, queuing time, and charging time of the EB fleet. The IA is implemented to solve the model, and the effectiveness of the approach is demonstrated by applying it to a real-world bus depot and four EB routes. The main conclusions are summarized as follows:

- (i) This paper collaboratively optimizes the number of charging piles in the bus depot and the charging plan of the EB fleet. The optimized charging pile deployment scheme reduces the number of charging piles by 4, thereby leading to cost savings of around 400,000 CNY as compared to the existing charging pile layout scheme in the bus depot.
- (ii) The charging performance of the battery is affected by the ambient temperature and the queuing time of EBs at bus depots, which influences the battery temperature at

the start of charging. The optimization method proposed in this paper can effectively control the queuing time of EBs at the bus depot, thereby realizing the improvement of the service efficiency of the bus depot without increasing the charging cost of the EB fleet. Additionally, it ensures the punctuality and integrity of the regional bus route operation.

- (iii) Given the time-of-use electricity price context, the optimized EB charging plan proposed in this study enables the charging time of the EB fleet to be concentrated in a specific time window. Compared to frequent multiple charging sessions, the plan minimizes the number of charging times and ensures that the battery SOC is closer to 50% at the beginning and end of charging. This approach is more favorable in terms of prolonging battery life.

Nevertheless, the concentrated charging approach has resulted in a significant issue of unequal usage of charging stations across various times of the day. Therefore, in the future, we intend to model the charging selection behavior of electric vehicles under different time periods or charging piles in the shared infrastructure scenario of EBs and private cars, and rationally design the number of charging stations and service fees to enhance the utilization rate of charging facilities and the revenue of bus companies.

**Author Contributions:** Conceptualization, J.W. and C.W.; methodology, J.W., H.W. and C.W.; software, J.W.; investigation, J.W.; validation, J.W., H.W. and C.W.; writing—original draft, J.W.; writing—review and editing, J.W., H.W. and C.W. All authors have read and agreed to the published version of the manuscript.

**Funding:** This research received no external funding.

**Data Availability Statement:** The authors confirm that the data supporting the findings of this study are available within the article.

**Conflicts of Interest:** The authors declare no conflict of interest.

## References

- Ji, J.; Bie, Y.; Wang, L. Optimal electric bus fleet scheduling for a route with charging facility sharing. *Transp. Res. Part C Emerg. Technol.* **2023**, *147*, 104010. [CrossRef]
- Global EV Outlook 2022. Available online: <https://www.iea.org/reports/global-ev-outlook-2022> (accessed on 13 May 2022).
- Csonka, B. Optimization of static and dynamic charging infrastructure for electric buses. *Energies* **2021**, *14*, 3516. [CrossRef]
- Battery Electric Buses—Things You Need to Know. Available online: <https://wendelcompanies.com/battery-electric-buses-things-you-need-to-know/> (accessed on 12 November 2019).
- Zhao, X.W.; Zhang, G.Y.; Yang, L.; Qiang, J.X.; Chen, Z.Q. A new charging mode of Li-ion batteries with LiFePO<sub>4</sub>/C composites under low temperature. *J. Therm. Anal. Calorim.* **2011**, *104*, 561–567. [CrossRef]
- Deng, R.; Liu, Y.; Chen, W.; Liang, H. A Survey on Electric Buses-Energy Storage, Power Management, and Charging Scheduling. *IEEE Trans. Intell. Transp. Syst.* **2021**, *22*, 9–22. [CrossRef]
- Paul, T.; Yamada, H. Operation and Charging Scheduling of Electric Buses in a City Bus Route Network. In Proceedings of the 2014 IEEE 17th International Conference on Intelligent Transportation Systems, Qingdao, China, 8–11 October 2014; pp. 2780–2786.
- Bie, Y.; Ji, J.; Wang, X.; Qu, X. Optimization of electric bus scheduling considering stochastic volatilities in trip travel time and energy consumption. *Comput. Aided Civ. Infrastruct. Eng.* **2021**, *36*, 1530–1548. [CrossRef]
- Ji, J.; Bie, Y.; Zeng, Z.; Wang, L. Trip energy consumption estimation for electric buses. *Commun. Transp. Res.* **2022**, *2*, 100069. [CrossRef]
- He, Y.; Liu, Z.; Song, Z. Optimal charging scheduling and management for a fast-charging battery electric bus system. *Transp. Res. Part E-Logist. Transp. Rev.* **2020**, *142*, 102056. [CrossRef]
- Hu, H.; Du, B.; Perez, P. Integrated optimisation of electric bus scheduling and top-up charging at bus stops with fast chargers. In Proceedings of the 2021 IEEE Intelligent Transportation Systems Conference, Indianapolis, IN, USA, 19–22 September 2021; pp. 2324–2329.
- Jiang, M.; Zhang, Y.; Zhang, Y.; Zhang, C.; Zhang, K.; Zhang, G.; Zhao, Z. Operation and scheduling of pure electric buses under regular charging mode. In Proceedings of the 2018 21ST International Conference on Intelligent Transportation Systems, Maui, HI, USA, 4–7 November 2018; pp. 1894–1899.
- He, Y.; Liu, Z.; Song, Z. Integrated charging infrastructure planning and charging scheduling for battery electric bus systems. *Transp. Res. Part D-Transp. Environ.* **2022**, *111*, 103437. [CrossRef]



14. Wang, G.; Fang, Z.; Xie, X.; Wang, S.; Sun, H.; Zhang, F.; Liu, Y.; Zhang, D. Pricing-aware real-time charging scheduling and charging station expansion for large-scale electric buses. *ACM Trans. Intell. Syst. Technol.* **2021**, *12*, 1–26. [\[CrossRef\]](#)
15. Liu, Y.; Wang, L.; Zeng, Z.; Bie, Y. Optimal charging plan for electric bus considering time-of-day electricity tariff. *J. Intell. Connect. Veh.* **2022**, *5*, 123–137. [\[CrossRef\]](#)
16. Bie, Y.; Hao, M.; Guo, M. Optimal electric bus scheduling based on the combination of all-stop and short-turning strategies. *Sustainability* **2021**, *13*, 1827. [\[CrossRef\]](#)
17. Zeng, Z.; Wang, S.; Qu, X. On the role of battery degradation in en-route charge scheduling for an electric bus system. *Transp. Res. Part E-Logist. Transp. Rev.* **2022**, *161*, 102727. [\[CrossRef\]](#)
18. Wang, Y.; Huang, Y.; Xu, J.; Barclay, N. Optimal recharging scheduling for urban electric buses: A case study in Davis. *Transp. Res. Part E-Logist. Transp. Rev.* **2017**, *100*, 115–132. [\[CrossRef\]](#)
19. Zhang, L.; Wang, S.; Qu, X. Optimal electric bus fleet scheduling considering battery degradation and non-linear charging profile. *Transp. Res. Part E-Logist. Transp. Rev.* **2021**, *154*, 102445. [\[CrossRef\]](#)
20. Fang, S.C.; Ke, B.R.; Chung, C.Y. Minimization of construction costs for an all battery-swapping electric-bus transportation system: Comparison with an all plug-in system. *Energies* **2017**, *10*, 890. [\[CrossRef\]](#)
21. Ding, H.; Hu, Z.; Song, Y. Value of the energy storage system in an electric bus fast charging station. *Appl. Energy* **2015**, *157*, 630–639. [\[CrossRef\]](#)
22. Zheng, F.; Wang, Z.; Liu, M. Overnight charging scheduling of battery electric buses with uncertain charging time. *Oper. Res.* **2022**, *22*, 4865–4903. [\[CrossRef\]](#)
23. Houbbadi, A.; Trigui, R.; Pelissier, S.; Redondo-Iglesias, E.; Bouton, T. Optimal scheduling to manage an electric bus fleet overnight charging. *Energies* **2019**, *12*, 2727. [\[CrossRef\]](#)
24. Jahic, A.; Eskander, M.; Schulz, D. Charging schedule for load peak minimization on large-scale electric bus depots. *Appl. Sci. Basel* **2019**, *9*, 1748. [\[CrossRef\]](#)
25. Bie, Y.M.; Tang, R.R.; Wang, L.H. Bus scheduling of overlapping routes with multi-vehicle types based on passenger OD data. *IEEE Access* **2020**, *8*, 1406–1415. [\[CrossRef\]](#)
26. Montoya, A.; Guéret, C.; Mendoza, J.E.; Villegas, J.G. The electric vehicle routing problem with nonlinear charging function. *Transp. Res. Part B Methodol.* **2017**, *103*, 87–110. [\[CrossRef\]](#)
27. Ke, B.R.; Chung, C.Y.; Chen, Y.C. Minimizing the costs of constructing an all plug-in electric bus transportation system: A case study in Penghu. *Appl. Energy* **2016**, *177*, 649–660. [\[CrossRef\]](#)
28. Bie, Y.; Liu, Y.; Li, S.; Wang, L. HVAC operation planning for electric bus trips based on chance-constrained programming. *Energy* **2022**, *258*, 124807. [\[CrossRef\]](#)
29. Gao, Z.H.; Xie, H.C.; Yang, X.B.; Niu, W.F.; Li, S.; Chen, S.Y. The dilemma of C-Rate and cycle life for lithium-ion batteries under low temperature fast charging. *Batter. Basel* **2022**, *8*, 234. [\[CrossRef\]](#)
30. You, H.Z.; Dai, H.F.; Li, L.Z.; Wei, X.Z.; Han, G.S. Charging strategy optimization at low temperatures for li-ion batteries based on multi-factor coupling aging model. *IEEE Trans. Veh. Technol.* **2021**, *70*, 11433–11445. [\[CrossRef\]](#)
31. Da Silva, S.L.E.F. Newton's cooling law in generalised statistical mechanics. *Phys. A Stat. Mech. Its Appl.* **2021**, *565*, 125539. [\[CrossRef\]](#)
32. Shah, K.; Drake, S.J.; Wetz, D.A.; Ostanek, J.K.; Miller, S.P.; Heinzl, J.M.; Jain, A. Modeling of steady-state convective cooling of cylindrical Li-ion cells. *J. Power Sources* **2014**, *258*, 374–381. [\[CrossRef\]](#)
33. Xun, J.; Liu, R.; Jiao, K. Numerical and analytical modeling of lithium ion battery thermal behaviors with different cooling designs. *J. Power Sources* **2013**, *233*, 47–61. [\[CrossRef\]](#)
34. Guo, Z.L.; Wang, S.; Zhuang, J. A novel immune evolutionary algorithm incorporating chaos optimization. *Pattern Recognit. Lett.* **2006**, *27*, 2–8. [\[CrossRef\]](#)
35. Chun, J.S.; Jung, H.K.; Hahn, S.Y. A study on comparison of optimization performances between immune algorithm and other heuristic algorithms. *IEEE Trans. Magn.* **1998**, *34*, 2972–2975. [\[CrossRef\]](#)
36. Vikram, S.; Vashisht, S.; Rakshit, D. Performance analysis of liquid-based battery thermal management system for Electric Vehicles during discharge under drive cycles. *J. Energy Storage* **2022**, *55*, 105737. [\[CrossRef\]](#)
37. Ma, Y.; Mou, H.; Zhao, H. Cooling optimization strategy for lithium-ion batteries based on triple-step nonlinear method. *Energy* **2020**, *201*, 117678. [\[CrossRef\]](#)
38. Ma, Y.; Li, J.Y. Iterative dynamic programming strategy for electric vehicle battery thermal management optimization. *Adv. Theory Simul.* **2022**, *5*, 2100602. [\[CrossRef\]](#)
39. Jana, A.; Shaver, G.M.; García, R.E. Physical, on the fly, capacity degradation prediction of LiNiMnCoO<sub>2</sub>-graphite cells. *J. Power Sources* **2019**, *422*, 185–195. [\[CrossRef\]](#)

**Disclaimer/Publisher's Note:** The statements, opinions and data contained in all publications are solely those of the individual author(s) and contributor(s) and not of MDPI and/or the editor(s). MDPI and/or the editor(s) disclaim responsibility for any injury to people or property resulting from any ideas, methods, instructions or products referred to in the content.